Isotopic evidence for the infiltration of mantle and metamorphic CO_2–H_2O fluids from below in faulted rocks from the San Andreas Fault system

É. Pili[1,2], B.M. Kennedy[3], M.E. Conrad[3], J.-P. Gratier[4]

[1]CEA, DAM, DIF, F-91297 Arpajon cedex, France
[2]Institut de Physique du Globe, Sorbonne Paris Cité, 1 rue Jussieu, 75238 Paris cedex 05, France
[3]Lawrence Berkeley National Laboratory, Berkeley, CA 94720, USA
[4]LGIT CNRS-Observatoire, BP 53, 38041 Grenoble, France

ABSTRACT

To characterize the origin of the fluids involved in the San Andreas Fault (SAF) system, we carried out an isotope study of exhumed faulted rocks from deformation zones, vein fillings and their hosts and the fluid inclusions associated with these materials. Samples were collected from segments along the SAF system selected to provide a depth profile from upper to lower crust. In all, 75 samples from various structures and lithologies from 13 localities were analyzed for noble gas, carbon, and oxygen isotope compositions. Fluid inclusions exhibit helium isotope ratios (^{3}He/^{4}He) of 0.1–2.5 times the ratio in air, indicating that past fluids percolating through the SAF system contained mantle helium contributions of at least 35%, similar to what has been measured in present-day ground waters associated with the fault (Kennedy et al., 1997). Calcite is the predominant vein mineral and is a common accessory mineral in deformation zones. A systematic variation of C- and O-isotope compositions of carbonates from veins, deformation zones and their hosts suggests percolation by external fluids of similar compositions and origin with the amount of fluid infiltration increasing from host rocks to vein to deformation zones. The isotopic trend observed for carbonates in veins and deformation zones follows that shown by carbonates in host limestones, marbles, and other host rocks, increasing with increasing contribution of deep metamorphic crustal volatiles. At each crustal level, the composition of the infiltrating fluids is thus buffered by deeper metamorphic sources. A negative correlation between calcite δ^{13}C and fluid inclusion ^{3}He/^{4}He is consistent with a mantle origin for a fraction of the infiltrating CO_2. Noble gas and stable isotope systematics show consistent evidence for the involvement of mantle-derived fluids combined with infiltration of deep metamorphic H_2O and CO_2 in faulting, supporting the involvement of deep fluids percolating through and perhaps weakening the fault zone. There is no clear evidence for a significant contribution from meteoric water, except for overprinting related to late weathering.

1. Introduction

A growing body of evidence suggests that fluids are intimately linked to a variety of faulting processes (see Hickman et al., 1995). This is particularly true for the plate bounding strike-slip San Andreas Fault (SAF) system, California, where it has been hypothesized that geo-pressured fluids impact the energetics of the system and weaken the fault with respect to shear failure. However, the role fluids play and their importance with respect to fault mechanics remains a topic of considerable debate (Scholz, 2000; Zoback, 2000). Models developed to explain the weakness of the SAF by means of high fluid pressures proposed different fluid sources. In the continuous flow model of Rice (1992), very high pore pressure is maintained in the fault zone by injection of geo-pressured fluids from the mantle. In the no-flow model of Byerlee (1990), water from the host rock is trapped in the fault zone where compressive forces raise the pressure of the trapped fluids above ambient hydrostatic pressure. If geophysics has provided indirect arguments for the potential role of fluids during seismogenic faulting (Johnson and McEvily, 1995; Unsworth et al., 1997; Zhao et al., 1996) such fluids have proven difficult to identify and sample (Kennedy et al., 1997; Wiersberg and Erzinger, 2007; Ali et al., 2010).

New approaches that can sample present-day fluids directly from recently ruptured fault zones either by sampling fluids during drilling (Wiersberg and Erzinger, 2007) or by extracting fluids from drilled cores (Shimamoto et al., 2001; Ali et al., 2010) are promising but limited in space and time. Fault zone minerals and fluid inclusions (fluids trapped in fractured minerals after healing or in secondary minerals after precipitation in fractures) associated with the active fault zones provide potential direct sampling of

fault-hosted fluid. Systematic variations in mineralogy and elemental or isotope chemistry in exposed fault zones compared to host rock compositions have long proved the involvement of fluids in faulting, and provide the means to decipher the nature, origin and flow paths of the fluids. Sampling rocks from the San Andreas Fault system for a geochemical and isotopic study of fluid–rock interactions is thus a promising approach for identifying the sources of fault zone fluids, their evolution in a still active system, and to establish further links with present-day fault parameters (locked or creeping segment, earthquake recurrence time, resistivity anomaly, energetics etc.) In a prior study of the Little Pine Fault, a segment of the SAF system, Pili et al. (2002) found that the influence of H_2O–CO_2 fluid mixtures and the alteration of the fault zone rocks increased towards the fault core. Evidence for two fluid sources, one internal and the other external, was also found and it was hypothesized that the external fluid was derived from deep metamorphism of the underlying Franciscan formation and the internal fluid was provided by a 30% volume reduction of the host limestones resulting from pressure solution and pore size reduction.

This paper presents a similar approach to that of Pili et al. (2002) but is applied at a much larger scale, encompassing most of the SAF system and incorporates helium isotope compositions to further constrain potential fluid sources. An early study of the chemistry of spring waters along the SAF (Irwin and Barnes, 1975) indirectly suggested the presence of metamorphic fluids in the fault zone, presumably contributed by underlying lithologies from the Franciscan formation, similar to the conclusion hypothesized for the more restricted study of the Little Pine Fault (Pili et al., 2002). A geographical coincidence between the H_2O, ^{18}O, and D content patterns of granitoid rocks and the trace of the SAF also supports the onset of water-rock interactions in the fault zone (O'Neil and Hanks, 1980). A pioneering but limited preliminary study of four shallow-depth cores drilled at one location on the SAF also suggested that metamorphic waters from adjacent Franciscan rocks migrated into the fault zone and mixed with local meteoric water in near surface sections of the fault (O'Neil, 1984). Profiles of soil–gas emanations across a trace of the SAF found evidence for focused flow of soil–gas CO_2 (Lewicki and Brantley, 2000). However, the CO_2 was dominated by shallow biogenic sources, masking any evidence for a deep component of CO_2 or enhanced flow from depth. Mantle-derived helium found in fluid samples from springs and wells associated with the SAF provided evidence for fluids from a mantle source that was presumed to enter the base of the seismogenic zone as a geo-pressured fluid capable of weakening the fault (Kennedy et al., 1997). Evidence for mantle-derived helium in fluids from the SAF system has been corroborated by three independent fluid studies conducted as part of the San Andreas Fault Observatory at Depth project (SAFOD, Hickman et al., 2004). Wiersberg and Erzinger (2007) found that drill mud-gas samples collected while drilling through the SAF system contained up to 12% mantle-derived helium at a depth of ~3.5 km. Ali et al. (2010) report similar helium isotope compositions in pore waters extracted from core taken while drilling though the SAF system. Evidence for mantle helium contributions to ground waters from the Mojave River Basin up to 35 km east from the SAF trace, has been reported by Kulongoski et al. (2003) and it was suggested that this helium influx originated from the SAF as well as other secondary fault zones in the basin.

These studies together with the results obtained by Pili et al. (2002) for a single SAF locality emphasize the need to decipher the relationships between the various fluids, their origins and their relationship to fault structures and processes. For this study, we have investigated the fluids involved in the faults using fault zone minerals and fluid inclusions across the SAF system. We present a comprehensive isotope study comparing gouges, fault planes, and vein fillings with their host rocks and the fluids associated with these materials, as sampled by fluid inclusions, over a major portion of the San Andreas Fault system, ranging from San Francisco to Los Angeles.

2. Geological setting and sampling localities

The San Andreas Fault system is a composite network of a large number of faults more or less active since 30 Ma, predominantly accommodating the right-lateral motion between the North American and Pacific plates (e.g. Wallace, 1990). We focused on three major fault zones that comprise the SAF system: faults associated with the San Gabriel Mountains, the Santa Ynez fault zone and the main strand of the SAF system from east Los Angeles north to San Francisco (Fig. 1). At the surface these sites expose a variety of lithologies from various depths of origin. The Santa Ynez and the San Gabriel fault subsystems (Fig. 1) are two former strands of the San Andreas Fault formed during the early development of the fault system. All of the studied fault segments have experienced displacements within the past 2 million years, but only the San Andreas segments have had displacement within historical time (Wallace, 1990).

We collected 75 samples from over 13 localities (Fig. 1). Sample localities and descriptions are given in Table 1, except for the Little Pine Fault samples, for which descriptions are given in Pili et al. (2002). Samples from the 3 sets of faults provide a depth profile of fluid–rock interactions from the upper to the lower crust. The Little Pine fault is a thrust fault adjacent to the Santa Ynez fault that is embedded in the Miocene Monterey (limestones) and the Cretaceous Franciscan (greywacke and serpentinites) formations (Dibblee, 1966) and represents the shallow upper crust. The main strand of the San Andreas Fault exposes a wide range of lithologies from unconsolidated sediments to metamorphosed rocks that represent the upper to middle crust. The San Gabriel fault, with its granitoids, anorthosites, and high-grade metamorphic rocks, is an exhumed middle to lower crustal equivalent of the SAF (Anderson et al., 1983).

In the field, faults are defined by damaged zones from 1 to 25 m wide, in some cases repeated two or three times with various spacing and decreasing width away from the fault core. These damaged zones are variously composed of gouges, fault planes, fault veins and veins. Fault planes, fault veins and gouges are altogether hereafter referred to as deformation zones by contrast with the vein (sealed cracks) and host rocks. In all types of faults, we sampled the major host rock lithologies, sedimentary, magmatic or metamorphic rocks:
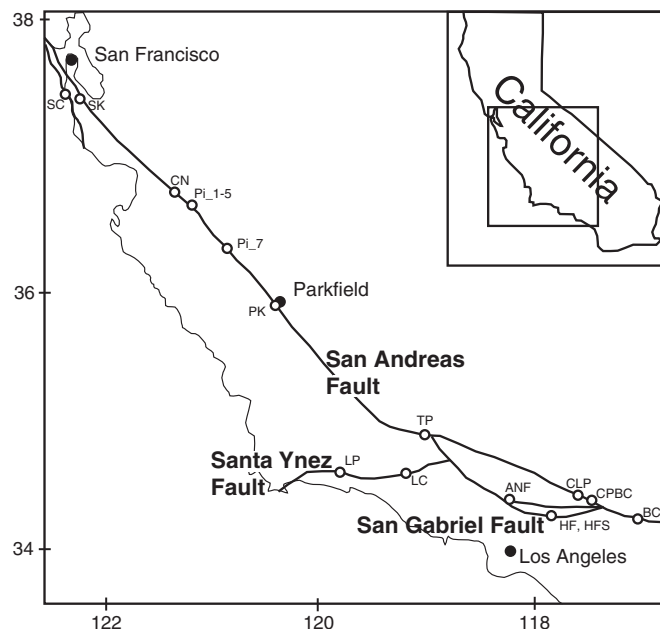

Fig. 1. Sampling area along the San Andreas Fault system with the names of the three major sets of faults: the Santa Ynez, the San Andreas (strictly speaking), and the San Gabriel faults. Open circles with abbreviations refer to sample locations (see Tables 1 and 2). Filled circles are reference localities.

Table 1
Sample description and carbonate[a] isotope compositions from deformation zones, veins and their host rocks.

Sample	Sample type (from field and thin section)	Setting[b]	% Carbonate	$\delta^{18}O$ (‰ SMOW)	$\delta^{13}C$ (‰ PDB)
Santa Ynez subsystem, Pine Fault at Lions Creek (LC; 34.57N, 119.15W)					
LC1H	Weathered sandstone	H	36	23.99	0.90
LC1V	Vein in sandstone (both weathered)	V	93	22.72	2.78
LC3VMdd	Fault vein in boulder within sandstone	V	89	22.25	-1.27
LC4WR	Matrix sandstone	H	28	21.81	-1.24
LC6H	Weathered sandstone	H	25	25.56	1.29
LC6Vdd	Vein in sandstone (both weathered)	V	74	24.71	1.38
San Andreas Fault, Cajon junction-Lone Pine Rd (CLP; 34.33N, 117.57W)					
CLP1H	Host marble	H	99	14.66	0.89
CLP1VM'	Carbonate vein in marble	V	85	13.45	0.66
CLP1VM	Carbonate vein in marble	V	17	13.82	0.25
CLP1MA	Carbonate slickensides (weathered)	D	90	20.15	-9.12
CLP2WR	Fault gouge in marble	D	70	13.09	0.78
CLP3WR	Marble	H	95	17.61	1.72
CLP4WR	Marble	H	94	14.85	1.49
CLP5WR	Granite	H	2	19.48	2.25
CLP5M	Carbonate slickensides in granite	D	2	13.22	-0.76
CLP6WR	Host marble	H	82	17.29	1.90
CLP6M	Carbonate slickensides in marble	D	97	12.09	1.99
San Andreas Fault, Cienega Road (CN; 36.73N, 121.36W)					
CN2	Host limestone	H	n.d.	20.30	2.38
San Andreas Fault, Cajon Junction-Blue Cut (CPBC; 34.26N, 117.46W)					
CPBC1H	Schist (weathered)	H	15	8.76	-11.45
CPBC2WR	Shear zone in schist	D	3	9.33	-2.64
CPBC3WR	Host schist	H	1	12.26	-2.74
CPBC5WR	Calcite vein in quartzite (weathered)	V	1	24.84	6.49
San Andreas Fault, Hw 25 from Hollister to Parkfield (Pi, PK)					
(Pi1 to Pi3; 36.68N, 121.26W)					
Pi1M	Carbonate slickensides (weathered)	D	24	25.90	-8.71
Pi1M1dd	Carbonate slickensides (weathered)	D	24	23.07	-9.29
Pi1M2dd	Carbonate slickensides (weathered)	D	54	23.66	-10.36
Pi1M3dd	Carbonate slickensides (weathered)	D	65	24.49	-14.12
Pi1WR2	Host limestone (weathered)	H	47	20.87	-6.48
Pi2WR	Host limestone	H	72	21.89	-0.57
Pi3WR	Host limestone	H	55	22.02	-0.40
(Pi4, Pi5; 36.61N, 121.21W)					
Pi4c	Sandstone (weathered)	H	28	23.91	5.58
Pi4V1	Vein in sandstone (weathered)	H	86	23.93	5.94
Pi4V2dd	Vein in sandstone (weathered)	H	96	23.90	5.49
Pi5cWR	Sandstone (weathered)	H	30	24.88	18.68
Pi5cWR	Shear zone in sandstone (weathered)	D	37	24.94	17.20
(Pi7; 36.31N, 120.92W)					
Pi7WR	Gouge in serpentinite	D	2	18.83	-2.15
Pi7V	Vein in serpentinite	V	65	19.41	-1.79
(PK samples; 35.90N, 120.43W)					
PK1Mdd	Fault plane (weathered)	D	39	28.20	-6.61
PK1WR	Gouge (weathered)	D	33	26.71	-5.33
PK2V2	Calcite vein in quartzite (both weathered)	V	38	24.92	0.48
PK3WR	Marble	H	56	15.37	-1.94
PK4WR	Marble	H	89	15.65	-0.36
PK5H	Quartz-carbonate layered rock	H	4	18.78	-5.50
PK5V	Vein	V	21	15.98	-5.57
PK6Vdd	Calcite vein in quartzite (both weathered)	V	91	28.47	7.89
PK8M	Carbonate slickensides (weathered)	D	40	26.62	8.06
PK8	Calcite vein in quartzite (both weathered)	V	8	25.30	7.08
PK9	Calcite vein in quartzite (both weathered)	V	7	24.73	9.33
PKII.1WR	Limestone	H	n.d.	18.30	-0.31
San Andreas Fault, Tejon Pass (TP; 34.80N, 118.88W)					
TP7	Limestone	H	n.d.	20.44	1.23
San Andreas subsystem, Pilarcitos Fault, Hw 92 (SK, 37.50N, 122.36W)					
SK1H	Host marble	H	91	19.68	-0.57
SK1V	Vein in marble	V	83	12.96	-3.72
SK2B1	Carbonate breccia clasts in psammite	D	96	14.21	-3.91
SK2B2	Carbonate breccia clasts in psammite	D	68	16.05	-1.51
SK2H	Host psammite	H	9	18.86	-0.63
SK2V	Vein	V	33	15.76	-1.18
SK3H	Host marble	H	57	19.64	0.37
SK3CV	2 cm wide vein in marble	V	100	13.61	-0.98
SK3V	1 mm wide vein in marble	V	88	13.66	-1.26
SK4WR	Shear zone in marble	D	32	14.59	-1.12

Table 1 (continued)

Sample	Sample type (from field and thin section)	Setting[b]	% Carbonate	δ^{18}O (‰ SMOW)	δ^{13}C (‰ PDB)
San Andreas subsystem, Pilarcitos Fault, Hw 92 (SK, 37.50N, 122.36W)					
SK5V1	Vein	V	94	19.37	0.26
SK5	Host marble	H	33	20.01	1.26
San Andreas subsystem, Seal Cove Fault at Moss Beach (SC; 37.52N, 122.52W) weathered siltstone from Pliocene Purisina Formation, foothill of a cliff on the shore					
SC2WR	Host siltstone outside of fault zone	H	67	24.71	5.30
SC3M-Calcite	Carbonate slickensides	D	92	31.11	22.55
SC3M-Dolomite	Carbonate slickensides	D	4	31.38	21.66
SC3M-TotCarb	Slickensides total carbonate[c]	D	96	31.12	22.51
SC3V-Calcite	Vein calcite	V	96	31.50	23.65
SC3V-Dolomite	Vein dolomite	V	4	31.38	21.66
SC3V-TotCarb	Total vein carbonate[c]	V	100	31.49	23.55
SC3WR-Calcite	Sheared host Siltstone calcite	D	13	31.77	22.58
SC3WR-Dolomite	Sheared host siltstone dolomite	D	1	31.07	21.55
SC3WR-TotCarb	Total siltstone carbonate[c]	D	14	31.72	22.51
SC3CQ	Fossil brachiopod shell		39	29.56	-3.06
San Gabriel Fault, Angeles National Forest, Big Tujunga Canyon Road (ANF; 34.28N; 118.21W)					
ANF3.1	Granite cataclasite	D	1	12.56	-7.60
San Gabriel Fault, Bear Creek (BC; 34.20N, 116.99W)					
BC2	Granite gouge	D	1	9.85	-7.97
San Gabriel Fault, Heaton Flat (river: HF, Shoemaker Canyon Road: HFS; 34.23N, 117.78W)					
HF2H	Mylonitic marble	D	43	10.26	-2.97
HF2V	Deformed vein in mylonitic marble	D	71	6.91	-3.90
HF3WR	Mylonitic gneiss with syn- to post-deformation calcite	D	3	9.95	-4.57
HF4WR	Mylonitic gneiss	D	3	13.28	-4.26
HF5WR	Mylonitic gneiss with syn- to post-deformation calcite	D	5	8.51	-5.15
HF6WR	Mylonitic gneiss with late-stage calcite vein	D	5	10.21	-5.10
HFS1WR	Gouge in granite	D	1	8.36	-8.30
HFS2	Carbonate slickensides in granite	D	4	13.42	-8.34
HFS4M	Carbonate slickensides in metabasalt	D	89	8.23	-7.72
HFS4V	Carbonate fault vein in metabasalt	D	87	6.66	-7.58
HFS5WR	Granite	H	4	11.53	-8.53

[a]Carbonate is calcite unless otherwise stated.
[b]D = deformation zone, V = vein, H = host rock.
[c]Total carbonate composition calculated from calcite and dolomite compositions and abundances.

sandstones, limestones, granitoids, basalts, serpentinites, gneisses, schists, and marbles. Gouges are a mechanical mixture of broken host rocks, mineral phases precipitated from interacting fluids, and host rock minerals that are recrystallized or destabilized. Gouges range from breccias to cataclasites or mylonites. In some granitic rocks, gouges are rich in chlorite and iron oxides and appear as dark layers (Chester et al., 1993; Evans and Chester, 1995). Fault planes are narrow zones of shearing which frequently expose polished surfaces with slickenfiber striations. Toward the fault plane, host rocks are increasingly brecciated; particle size (rock pieces or minerals) decreases, and the amount of reworked material increases with increasing amounts of mass transfer as commonly shown by calcite or quartz precipitates. Fault veins also developed parallel to fault planes by sealing of cracks and present slickenfiber striations. Veins developed as fractures during earthquakes or during the related interseismic deformation since their orientation are consistent with neighboring fault displacements. A comprehensive study of the geochemical and structural relationships between veins, gouges and host rocks is given by Pili et al. (2002) and is modeled by Gratier et al. (2003).

We systematically sampled deformation zones, veins and host rocks across and along fault zones, with centimeter- to kilometer-scale profiles. Finding a pristine host rock to be compared with deformation zones proved to be difficult in regionally deformed terrains, particularly in high-grade metamorphic conditions. Calcite fills most of the veins and deformation zones. Quartz may rarely be found with calcite in the same veins. Abundant fluid inclusion trails (sealed micro-cracks) parallel veins in host minerals. Primary fluid inclusions may be present in quartz and calcite corona growth in some veins.

3. Noble gases from fluid inclusions: Analytical methods and results

The samples were first coarsely crushed, sieved and a coarse grain fraction (1–5 mm) was separated for noble gas analyses. Quasi-monomineralic samples were used in most cases to obtain pure coarse grain fractions. Minerals were separated by hand-picking, ultrasonically washed in methanol, acetone and ethanol, then air dried. Noble gases were extracted from ~1 g samples of the quartz and/or calcite separates by crushing under high vacuum. Crushing mostly releases noble gases from inclusions and is used to separate occluded noble gases from noble gases residing within the mineral matrix, such as in situ produced radiogenic and cosmogenic isotopes (e.g. Brook and Kurz, 1993). However, redistribution of noble gas species between matrix and inclusions by diffusive processes cannot be completely ruled out. Therefore, for this project, we cautiously operated under the canonical view that crushing primarily releases noble gases that were trapped in inclusions during mineral growth (e.g. Ballentine et al., 2002; Stuart et al., 1994). Purification and analyses of the released gases follow Dodson et al. (1997). Results are presented in Table 2 for helium concentrations ([^{4}He] in 10^{-9} cm^3 g^{-1}), helium isotope compositions (given as R/Ra, where R is the ^{3}He/^{4}He ratio in the sample normalized to the same ratio in air, Ra ~ 1.4 10^{-6}) and relative abundances [F(^{4}He)], defined as the ^{4}He/^{36}Ar ratio in the sample normalized to the same ratio in air (0.167). The sample data have been corrected for sample preparation line blank determined using the same procedures applied to the samples and for analytical fractionation, by normalization to repeated measurements of air and helium standards. The later has a ^{3}He/^{4}He ratio of 2.4 Ra. The

Table 2
Noble gas isotope compositions from fluid inclusions and modeled reservoirs.

Sample	Sample type[a]	Host mineral		Outcrop	$[^4He]$ 10^{-9} cm^3g^{-1}	R/Ra[b] $\pm 1\sigma$	$F(^4He)$[c]
*Santa Ynez Fault system, Little Pine Fault (LP; 34.54N, 119.75W)**							
LP1	Weathered peridotite	D	Olivine	River bank	0.09	Blank bound	8.78
LP2H	Sheared greywacke	D	Quartz	–	0.82	1.19 ± 0.32	29.48
LP2V	Slickensides in greywacke	D	Quartz	–	2.73	0.76 ± 0.20	9.72
LP4M	Carbonate gouge	D	Calcite	–	0.83	1.44 ± 0.35	1.85
LP10V	Carbonate vein	V	Calcite	–	3.77	0.62 ± 0.13	5.45
LP15V	Carbonate vein	V	Calcite	–	1.32	0.83 ± 0.14	3.91
LP17V	Carbonate vein	V	Calcite	–	3.73	1.40 ± 0.25	16.21
San Andreas Fault							
CLP2	Gouge	D	Calcite	Road cut	1.65	0.54 ± 0.11	11.26
CPBC1V	Weathered quartz vein	V	Quartz	–	0.14	0.14 ± 0.05	1.31
CPBC1H	Weathered schist	H	Quartz	–	1.24	0.80 ± 0.12	3.48
PK2	Weathered quartzite	H	Quartz	Ridge crest	3.47	0.10 ± 0.03	9.30
PK3	Marble	H	Calcite	–	21.11	0.34 ± 0.04	49.48
PK8	Weathered quartzite	H	Quartz	Eroded surface	3.78	0.41 ± 0.17	6.61
PK13	Highly veined chert	D	Quartz	–	0.22	1.84 ± 0.49	4.28
San Andreas Fault subsystem, Pilarcitos Fault							
SK1V	Carbonate vein	V	Calcite	Quarry	15.08	0.45 ± 0.07	68.85
SK5	Marble	H	Quartz	–	0.60	1.45 ± 0.42	0.55
San Gabriel Fault							
HF2	Marble mylonite	D	Calcite	River canyon	0.89	Blank bound	6.68
HF6	Quartz–chlorite mylonite	D	Quartz	–	0.16	2.53 ± 0.80	1.83
Air saturated water						1.00	0.26
Crust						0.02	100
Mantle						8	100

[a] D = deformation zone, V = vein, H = host rock.
[b] R/Ra is the $^3He/^4He$ ratio in the sample compared to the same ratio in air (Ra~1.384 10^{-6}).
[c] F(^4He) is the $^4He/^{36}Ar$ ratio of the sample compared to the same ratio in air.
*Associated $\delta^{13}C$-$\delta^{18}O$ values from Pili et al. (2002).

reproducibility of the air standard $^4He/^{36}Ar$ ratio is ±6% (1σ) and the reproducibility of the $^3He/^4He$ ratio for the helium standard is ±5% (1σ). In general, gas concentrations were low and in two cases indistinguishable from blank. The given $^3He/^4He$ ratios have not been air-corrected. This correction does not change the presented results.

The distribution of the fluid inclusion helium isotope compositions from the quartz and calcite separates are summarized in Fig. 2. The helium compositions range from 0.10 ± 0.03 to 2.53 ± 0.80 (1 σ). $^3He/^4He$ ratios show a similar distribution for host rocks (0.10–1.45) and veins (0.14–1.40), but increase in deformation zones (0.54–2.53). The distribution of the fluid inclusion helium isotope compositions

displays a similar range as that measured in present-day fluids associated with the SAF (Kennedy et al., 1997; Wiersberg and Erzinger, 2007; Ali et al., 2010). In terms of fault segments, the highest R/Ra value was observed in a San Gabriel fault sample (2.53 ± 0.80), followed by a San Andreas fault sample (1.84 ± 0.49), and a Santa Ynez one (1.44 ± 0.35). In deformation zones the highest helium ratios are found in quartz (0.76–2.53 Ra) compared to calcite R/Ra of (0.54–1.44 Ra). The lowest He ratio (0.10 Ra) was measured in a weathered quartzite host rock from the SAF segment in Parkfield.

4. Stable isotopes: Analytical methods and results

Carbonates are frequently found in host rocks, in veins, and in deformation zones. This is a suitable mineralogy when comparing isotope compositions of faulted rocks and their hosts. In addition, carbonate analyses lead to two isotopic compositions, $\delta^{13}C$ and $\delta^{18}O$, which are of great help when deciphering H_2O–CO_2 fluid–rock interactions. As carbonates are the major minerals in limestones and marbles, these lithologies have been abundantly sampled and analyzed in this study, but the same isotope ratios in carbonates from other lithologies (sandstones, quartzites, schists and granites) also proved to be fruitful.

Carbon and oxygen isotope analyses are reported as per mil (‰) variations with respect to VPDB and VSMOW standards, respectively. Isotopic compositions and yields for carbonate were measured on CO_2 gas extracted through reaction with H_3PO_4 following the technique outlined by Sharma and Clayton (1965). Calcite-rich samples were analyzed using an automated carousel system by reacting the samples at 90 °C for 12 min. Samples poor in calcite or mixed calcite-dolomite samples were reacted at 25 °C for 1–5 days with manual extraction of the CO_2 from the reacted samples on a vacuum line. However, as the dolomite content was <6%, isotope measurements from automated carousel extractions and manual extractions (after bulk carbonate content recalculation) agree within 0.2‰. Precision for the analyses is
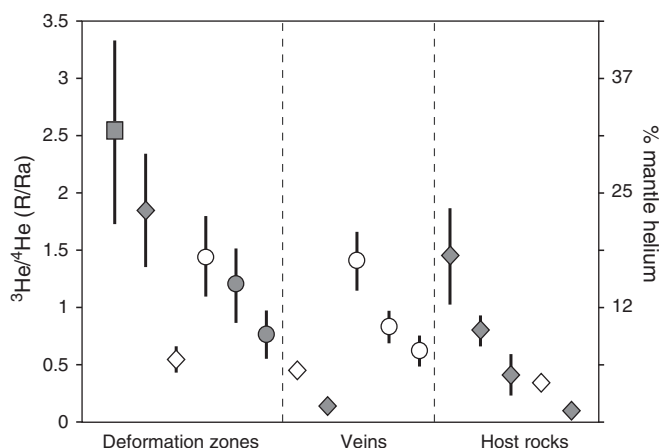

Fig. 2. Distribution of the helium isotope ratios ($^3He/^4He = R$) normalized to air (R/Ra, Ra = 1.384 10^{-6}) from fluid inclusions hosted in quartz (gray symbols) and calcite (white symbols) minerals taken from deformation zones, veins, and host rocks, from the San Gabriel (squares), the San Andreas (diamonds), and the Santa Ynez (circles) faults. Associated mantle helium contribution (atom %) calculated as described in text, section 5.3.

±0.05‰ for carbon and ±0.1‰ for oxygen. The carbon- and oxygen-isotope compositions of carbonates from hosts, veins, and deformation zones are presented in Table 1 and in Fig. 3. Carbon- and oxygen-isotope analyses from limestones sampled across the Little Pine fault are reported in Pili et al. (2002). These analyses were conducted with the same method as for the present study. The data are included in Fig. 3. The main data features are presented below for the three main fault subsystems.

The carbon and oxygen isotopic compositions for the entire data set have a large range of compositions: $7‰ < \delta^{18}O < 27‰$ and $-9‰ < \delta^{13}C < 5‰$ (Fig. 3). Despite the large range, there is a general positive correlation between $\delta^{13}C$ and $\delta^{18}O$. Samples from deformation zones are characterized by the lowest isotopic compositions, host rocks have the highest compositions while vein minerals are intermediate between deformation zone and host rock compositions.

Carbonate samples from the San Andreas Fault were collected from a range of sedimentary and metamorphic lithologies (Table 1). C-O isotope ratios for limestone host rocks are lower ($-1‰ < \delta^{13}C < 2‰$ and $18‰ < \delta^{18}O < 22‰$) than for similar lithologies from the Santa Ynez Fault. Vein and deformation zone compositions are lower than the host limestone by up to 4‰ for carbon and up to 7‰ for oxygen. Marbles have $\delta^{18}O$ and $\delta^{13}C$ in the range 14–20‰ and -2 to 2‰, respectively. Vein and deformation zone compositions are lower by up to 3‰ for carbon and up to 7‰ for oxygen than the host marble. In the Pelona formation (samples CPBC, Table 1), as for other rocks from Parkfield (PK5 series), the deformation zone carbonates have $\delta^{18}O$ values 3‰ lower than the host rocks but similar $\delta^{13}C$ values. Compositions of carbonate slickensides are lower by 6% for oxygen and 3% for carbon compared to their host granite (CLP5).
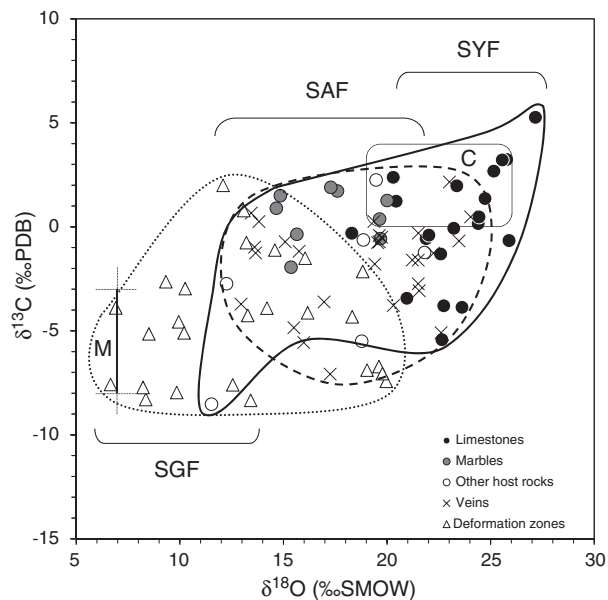
Fig. 3. Carbon- and oxygen-isotope compositions of carbonate minerals from the San Andreas Fault system, for host rocks, veins and deformation zones. Host rock compositions are reported for limestones (black dots; after Pili et al. (2002) and this study), marbles (gray dots), and other rocks (open circles, see their lithologies in Table 1). Fields are drawn for host rocks (solid line), veins (dashed line) and deformation zones (dotted line). Two end-member compositions are reported: C (rectangle), typical pristine crustal limestone; M: carbonates of mantle derivation (Javoy et al., 1986). The overall C- and O-isotope compositions of the various carbonated host rocks follow a trend with decreasing $\delta^{13}C$ and $\delta^{18}O$ values that goes with increasing amount of carbonate of metamorphic or mantle origins in these rocks. This trend also matches the increasing depths of exposure for, respectively, the Santa Ynez (SYF), the San Andreas (SAF), and the San Gabriel (SGF) faults from the upper crustal level down to the lower crustal level. The isotope compositions of carbonate from veins and deformation zones follow the same trend, indicating infiltration by deep crustal, metamorphic or mantle H_2O–CO_2 fluids.

Carbonate samples from the exhumed San Gabriel Fault were extracted from various metamorphic rocks, including marble, gneiss, granite, and metabasalt (Table 1). Deformation is widespread and lithologies are heterogeneous, thus host rocks were not easily distinguished from deformation zone rocks at more than the centimeter-scale making comparison difficult. Granites yielded from 1 to 4% of calcite consisting of disseminated minerals, fracture filling material or cement in cataclasites. This mass transfer is evidence for infiltration by external fluids. Veins were also difficult to sample as they are often highly deformed. Only late-stage veins crosscutting the overall deformation pattern could be clearly isolated and are reported here. The C-O isotope systematics for host rocks, deformation zones and veins from marble, gneiss, granite, and metabasalt from the San Gabriel Fault differs from those found in the other fault zones. The composition of sample HF2 (Table 1), from a deformation zone, is lower by 3‰ for oxygen and 0.9‰ for carbon compared to its host marble. Syn- to post-deformation calcite in mylonitic gneiss demonstrate a range of compositions ($8.5‰ < \delta^{18}O < 10‰$ and $-5‰ < \delta^{13}C < -4.5‰$), while late-stage calcite veins are characterized by relatively constant compositions ($\delta^{18}O \sim 10‰$ and $\delta^{13}C \sim -5‰$).

As shown in Fig. 3, the overall C- and O-isotope compositions of carbonates from the various host rocks (limestones, marbles, gneisses and granites) follow a general trend of decreasing $\delta^{13}C$ and $\delta^{18}O$ values. This trend coincides with the fault subsystem (Santa Ynez > San Andreas > San Gabriel faults), and with the associated depth profile of fluid–rock interactions from the upper to the lower crust. The isotope compositions of carbonate from veins and deformation zones follow these same trends. Furthermore, the isotope fractionation between veins or deformation zones and their respective host rocks decrease for samples from increasing original depths.

Before further discussion of the observed isotopic trends, it is important to evaluate the possible impact of weathering on the isotopic compositions of interest. This was accomplished by collecting obviously altered/weathered samples and comparing the isotopic compositions of the very first few outer millimeters of sample surfaces extracted using a dental drill to their core compositions. By this method we intended to document only weathering and no other diagenetic or hydrothermal processes that could have modified the whole rock composition prior to faulting. In carbonate-rich rocks, as shown in single hand-specimens of marble and limestone (see samples CLP1 and Pi1, Table 1), carbon and oxygen isotope shifts due to weathering are large, up to -9‰ for carbon and +5‰ for oxygen. Compared with non-weathered samples, in a $\delta^{13}C$ vs. $\delta^{18}O$ diagram (Fig. 4), these compositions plot in a different domain and these shifts form a trend perpendicular (i.e. increasing $\delta^{18}O$ with decreasing $\delta^{13}C$) to the one observed for deformation zones, veins and their hosts (Fig. 3). Weathering is especially important on exposed fault plane surfaces, but may also affect host rocks deeper. A typically weathered host limestone sample (Pi1WR2, see Table 1) as shown in thin section, has a marked $\delta^{13}C$ shift of around -6‰ compared to non-weathered limestones nearby (Pi2WR and Pi3WR). Weathering in carbonate-rich lithologies tends toward a well defined oxygen-isotope composition with $\delta^{18}O \sim 25‰$ and decreasing $\delta^{13}C$ values. Weathering in carbonate-poor rocks (quartzites, sandstones, silt-stones) also exhibits distinctive C- and O-isotope compositions (Fig. 4). Weathered quartzites show conspicuous carbonate veining with $25 < \delta^{18}O < 28‰$ and $0 < \delta^{13}C < 9‰$, whereas matrix carbonate from weathered sandstones have $\delta^{18}O$ of 24–26‰ and $\delta^{13}C$ of 1–19‰. Compared to carbonate-rich lithologies, weathering in carbonate-poor lithologies also tends to have oxygen isotope composition at $\delta^{18}O \sim 25‰$ with increasing $\delta^{13}C$ values.

5. Discussion

The existence of fracture fillings with fluid inclusions, their relations with faults, as well as the noble gas and stable isotope
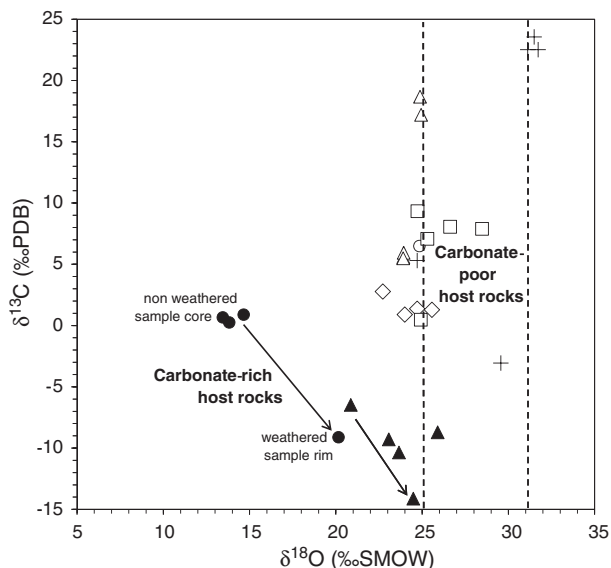
Fig. 4. Plot of the carbon- and oxygen-isotope compositions of carbonates from weathered rock samples from the San Andreas Fault (see text, sections 4 and 5.1, as well as Table 1 for details). Weathering is observed independently in host rocks, veins and deformation zones. Two distinct fields are observed for samples taken either in carbonate-poor (silica-rich, open symbols) or carbonate-rich (solid symbols) host rocks. The two arrows depict compositions of sub-samples from least to most weathered, taken out with a dental drill, from core to rim respectively, within millimeters of two samples (a marble and a limestone). Weathering results in marked O-isotope compositions: the vertical dashed lines stand for carbonate compositions in equilibrium with meteoric water ($\delta^{18}O\sim25‰$) and oceanic water ($\delta^{18}O\sim31‰$), respectively, for temperatures in the range 10–20 °C. Sample series as follows (see in Table 1 samples mentioned as weathered): black dots: CLP1; black triangles: Pi1; white triangles: Pi4 and Pi5, diamonds: LC1 and LC6; squares: PK2, PK6, PK8, PK9, open circles: CPBC5; crosses: SC2, SC3.

compositions of deformation zones, veins and host rocks, show that fluid infiltrations occurred while the fault were active. The origins of the infiltrating fluids, and the mechanisms by which the fluids enter and migrate into the San Andreas Fault system can be documented from the present isotope study.

5.1. Weathering and low-temperature meteoric water are not involved in the stable isotope compositions of the analyzed faulted rocks

Weathering (action of meteoric water, seawater, and atmospheric or biospheric agents at temperature<40 °C) must be well characterized when one deals with fluid–rock interactions. It is well-known that outcrops of consolidated sediments, metamorphic and magmatic rocks are rare along the SAF system due to the general lack of relief and small differential erosion rates. Indeed, the faults are mainly expressed in unconsolidated Quaternary alluvium. Also, vegetation cover or microbial activity may hamper proper sampling. The lack of fresh rock outcrop can lead to the sampling of weathered rocks in which possible other types of fluid–rock interactions may have become blurred. In order to determine whether or not meteoric water significantly infiltrated the SAF system it is of great importance to characterize any possible surface weathering of the rock samples because the effects of surface weathering of rock must not be confused with the effects of meteoric water infiltration into fault zones.

As shown in Fig. 4, weathering is characterized in most carbonates by a nearly constant $\delta^{18}O$ around 25‰ and two distinct families of $\delta^{13}C$ values, one with low values ($\delta^{13}C<-5‰$) for carbonate-rich rocks, the other with high values ($-6‰<\delta^{13}C<24‰$) for carbonate-poor (silica-rich) rocks. The $\delta^{18}O$ value of about 25‰ coincides with the isotope composition of calcium carbonate in equilibrium with meteoric water along the San Andreas fault ($\delta^{18}O$ water around -6‰, from White et al., 1973; O'Neil, 1984; Kennedy et al., 1997;

Melchiorre et al., 1999) for a reasonable temperature (10–20 °C) and fractionation factor from O'Neil et al. (1969). Carbonate matrix from weathered siltstones cut off from a cliff under ocean brine influence show extreme isotope compositions with $\delta^{18}O$ of about 31‰ and $\delta^{13}C$ of about 22‰ (sample series SC3, Table 1, and Fig. 4). Veins and host have here similar compositions which suggest pervasive infiltration and late overprint. A single centimetric fossil brachiopod shell extracted from one of these weathered siltstones yielded $\delta^{13}C = -3‰$ and $\delta^{18}O = 30‰$. In this case, the $\delta^{18}O$ value of about 30‰ or 31‰ coincides with the isotope composition of calcite in equilibrium with oceanic water at a temperature in the range 10–20 °C and fractionation factor of O'Neil et al. (1969).

Sub-samples of carbonate rocks taken with a dental drill from the core to the rim of the sample show a trend towards lower $\delta^{13}C$ and $\delta^{18}O$ of about 25‰. For all the carbonate-poor samples whatever their origins, the narrow range in $\delta^{18}O$ values (~24–31‰) for a large range in $\delta^{13}C$ values (0–24‰) is consistent with a trend controlled by the $\delta^{18}O$ of the infiltrating water (dashed lines in Fig. 4). For carbonate-rich as for carbonate-poor lithologies, the oxygen isotope compositions of carbonates therefore seems to be controlled by the weathering fluid, whether it is meteoric or oceanic water. Contrasting values of $\delta^{13}C$ for carbonate-rich and carbonate-poor lithologies suggest that the carbon mass-balance rules the process of carbonate weathering. Whereas the $\delta^{13}C$ values of precipitated carbonates are solely inherited from the fluid in carbonate-poor lithologies, the $\delta^{13}C$ values are partially derived from the host rock in carbonate-rich lithologies, either via isotope exchange with a fluid or chemical reactions such as devolatilization. Extreme $\delta^{13}C$ values imply large fractionations possibly due to the involvement of a gas phase such as CO_2 or CH_4 and/or a link with microbial activity.

The isotope trends observed for weathering (Fig. 4) are at odds with the general trends observed in the fault deformation zones, veins and their host rocks (Fig. 3). Although some of the scatter in Fig. 3 data may be related to weathering effects, the overall general trend cannot be driven by weathering. Therefore, the fluid–rock interactions found in faulted rocks in the present study can be attributed unambiguously to fluid infiltrations that occurred during faulting.

5.2. Metamorphic fluid sources infiltrated from below in the San Andreas Fault system

The fluids that have infiltrated the San Andreas Fault system are a mixture of H_2O and CO_2. This is shown by (1) the secondary carbonated and hydrous secondary minerals (calcite, serpentine, clay minerals) filling fractures or replacing primary minerals and by (2) the correlated carbon- and oxygen-isotope shifts in carbonates from host rocks, veins and deformation zones (Fig. 3).

Methane (CH_4) and hydrogen (H_2) are two gases commonly reported to emanate from fault zones (i.e. Sugisaki et al., 1980) and some of the SAFOD fluids collected during drilling (Erzinger et al., 2004; Wiersberg and Erzinger, 2008). However, evidence for these reduced gases has not been found in our study. Methane infiltration instead of CO_2 would result in markedly different fractionation factors for ^{13}C (e.g. Friedman and O'Neil, 1977), and would only affect the carbon not the oxygen-isotope systematics. However, methane and hydrogen gas have been suggested as possible precursors of seismic events (see the review of Toutain and Baubron, 1999). They could be generated on a very local scale from CO_2 and H_2O fluids through reducing reactions on highly reactive mineral surfaces that just ruptured (Kita et al., 1982). Methane observed in drill mud-gas during drilling of the SAFOD Pilot Hole is attributed to a mixture of microbial and thermogenic origins (Erzinger et al., 2004; Wiersberg and Erzinger, 2008).

The overall C- and O-isotope compositions of the carbonate host rocks analyzed for this project (limestones, marbles, gneisses and granites) follow a trend of decreasing $\delta^{13}C$ and $\delta^{18}O$ values with

increasing amount of metamorphic carbonate in the rocks. This trend also matches the increasing depths of exposure for the Santa Ynez, San Andreas, and San Gabriel faults from the upper crust toward the lower crust. The isotope compositions of carbonate from veins and deformation zones follow the same trend, indicating a deep origin for the H_2O–CO_2 fluid infiltrated during faulting. In addition, the isotope fractionations between veins or deformation zones and their host rocks decrease for samples from increasing depths. Therefore, with increasing depth, fluids and rocks approach equilibrium (fluids get closer in composition to those that may have originated from these rocks), or the isotope fractionations between the precipitated minerals and the fluid decrease (fluid temperature increases) or both, indicating again that the H_2O–CO_2 fluids are of deeper origin, being at each crustal level hotter than their hosts and at equilibrium with deeper rocks of a higher metamorphic grade.

A deep metamorphic fluid has also been hypothesized based on the stable isotope and trace element constraints presented in the Pili et al. (2002) study of the Little Pine Fault (Santa Ynez subsystem) where metamorphism of the deeper underlying Franciscan formation provides an external fluid source. Indeed, with $19 < \delta^{18}O < 25$‰ and - $9 < \delta^{13}C < $-3‰ (Magaritz and Taylor, 1976), carbonates from various lithologies of the Franciscan Formation represent an end-member for carbonate compositions from the Little Pine Fault (SYF, Fig. 3). CO_2 derived from metamorphism has also been hypothesized by Wiersberg and Erzinger (2007) and Wiersberg and Erzinger (2008) in their study of SAFOD fluids. The $\delta^{13}C$ data most likely indicate a source of carbon derived from organic-rich shales and permeable sandstones drilled in the lower sedimentary section of the SAFOD Main Hole. Moore and Rymer (2007) also observed that talc is forming as a result of the reaction of serpentine minerals with silica-saturated hydrothermal fluids that migrate up the fault zone. Therefore, for fault segments suspected to be particularly hazardous, the potential of their host lithology to produce metamorphic fluids should be evaluated in order to take into account the role of possible fluid infiltrations in triggering a seismic event.

5.3. Mantle-derived fluids identified in faulted rocks from the SAF

The isotopic composition and relative abundance of helium can provide unequivocal evidence for fluid sources in crustal hydrologic systems. This is demonstrated in Fig. 5 where the fluid inclusion helium isotopic data (R/Ra) is plotted as a function of the helium relative abundance or enrichment factor [F(^{4}He)]. Most noteworthy is the large difference in isotopic composition between canonical crustal (0.02 Ra) and MORB-mantle (8 Ra) end-members, providing a very sensitive tracer for mantle and crustal fluid input to a hydrologic system. For the SAF system, the specific helium relative abundance for the crustal and mantle end-members is not known. However, universally, these end-members have been found to be strongly enriched in helium and in present-day fluid samples associated with the SAF system F(^{4}He) values up to >1000 have been observed (Kennedy et al., 1997). For the purpose of discussion, we have assumed an arbitrary F(^{4}He) for the crust and mantle end-members of 100 and have constructed mixing curves (e. g. Albarède, 1995) between the crustal end-member and air or air saturated water [F(^{4}He) <1, R/Ra = 1] and the mantle end-member and air or air saturated water (Fig. 5). The salient result is that almost all of the samples are (1) enriched in ^{4}He with respect to air or air saturated water and (2) must contain ^{3}He that cannot be accounted for by crustal or atmospheric sources alone.

Possible sources for the excess ^{3}He are mantle infiltration or cosmogenic production during surface exposure. The former is trapped in the inclusions during mineral growth and the later added to the inclusion hosted inventory by subsequent diffusion from the quartz and calcite matrices (e.g. Brook and Kurz, 1993). Five of the samples (CLP2, CPBC1-H and –V, SK1 and SK5, Table 2) were collected from recently exposed quarry walls or road cuts rendering cosmo-
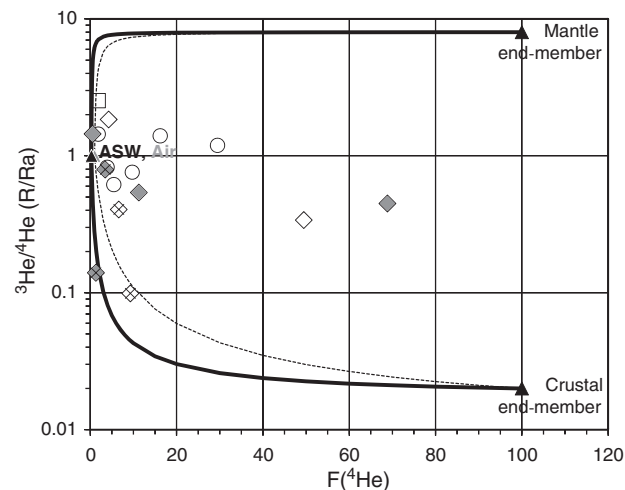

Fig. 5. Plot of the fluid inclusion helium isotopic compositions (R/Ra) as a function of the helium enrichment factors [F(^{4}He)] (see Table 2). Dots: LP samples, Little Pine Fault, Santa Ynez subsystem; diamonds: CLP, CPBC, PK and SK samples (gray when taken from quarries or road cuts, with a cross when weathered), San Andreas Fault; square: HF6 sample, San Gabriel Fault. The two triangles on the left stand for compositions of Air Saturated Water and Air, respectively. The curves depict mixing between air saturated water (solid line) or air (dashed line) and mantle or crustal end-member reservoirs defined by their respective helium isotopic compositions and an assumed helium enrichment factor of 100. Note that the form of the mixing lines is insensitive to this assumption, as long as the enrichment factors are greater than ca. 20. Since most of the data plot between the mixing curves, the fluid inclusions must contain mantle and crustal-derived helium.

genic contributions insignificant thus requiring a mantle source for the excess ^{3}He for three of the samples (Fig. 5). The two other samples (CPBC1-H and –V, both weathered) lie near the crust-air or crust-air saturated water mixing lines, in the same manner as the two other weathered samples (PK2 and PK8). Cosmogenic ^{3}He contamination of trapped fluids is expected to be more important in rocks exposed for a long time at the surface. These same rocks would be the most likely to experience significant weathering. However, our weathered samples do follow the air–crust mixing line in Fig. 5, indicating the absence of a significant contribution of cosmogenic ^{3}He.

The extent of a potential cosmogenic He contamination in fluids trapped in inclusions may be estimated from a simple geometrical perspective. Considering 1000 spherical fluid inclusions with a radius of 10 μm trapped within a spherical grain with a radius of 1 mm, they occupy 0.1% of the grain volume while their total internal surface area represents 10% the external surface area of the grain. As He diffusion is expected to occur similarly from the crystal toward the inclusions or toward the outside of the grain, the loss of He outside the grain is expected to be 1 order of magnitude higher than the contamination of fluid trapped in inclusions, without considering He concentration gradients. Fluid inclusions must occupy 10% of the grain volume in order to lead to an inward flux of ^{3}He in the inclusion higher than an outward loss from the grain boundary.

Following Pik and Marty (2009), who similarly discussed the use of helium measurements in calcites to infer the nature of fluid flow in faulted rocks, the offset observed between the composition measured in our samples and the air–crust or ASW–crust mixing lines drawn in Fig. 5 could be explained by addition of cosmogenic ^{3}He corresponding to exposures of 200–2000 years (computed with a production rate of ~110 atom g^{-1} year $^{-1}$, e.g. Vermeesch et al., 2009). If these durations can be excluded for samples taken from quarry walls or road cuts, this could be the same for all of our samples, since they are taken from the trace of the SAF, where vertical movement associated with creeping or seismic rupture (Zoback et al., 1987) is likely to lead to uplift and erosion on short time-scales. In addition, no relation between the ^{3}He/^{4}He ratios and the amount of

[3]He is observed for our samples, which would be the case for fluid inclusions contaminated by cosmogenic He (Brook and Kurz, 1993). Moreover, as discussed below, correlations between helium and carbon isotopic compositions that are consistent with mantle contributions provide a strong argument against significant cosmogenic overprinting of the inclusion noble gas inventory. Given this, we cautiously proceed under the assumption that the inventory of excess [3]He is dominated by contributions from the mantle.

Within the constraints of the mixing lines depicted in Fig. 5, the fractional contribution of each end-member to a sample composition can be calculated. However, given the uncertainties in the measured compositions and the assumed end-member compositions, a rigorous calculation would seem unwarranted. Nevertheless, using the assumed end-members, the mantle contribution to the fluid inclusion helium data varies from ~0% (SAF sample CPBCIV, weathered quartz vein) to ~35% (SGF sample HF6, deformation zone quartz). The maximum helium contribution for each SAF subsystem suggests the following hierarchy SGF>SAF>SYF, consistent with the relative fault zone depths at which the fluid inclusions were presumably trapped in their host minerals.

It has been observed that in mantle fluids CO_2 and [3]He occur in a nearly constant proportion to each other, suggesting that mantle-derived CO_2 is a likely carrier phase for the trace helium component (e.g. Marty and Jambon, 1987; Polyak et al., 2000). The presumed presence of mantle-derived helium in fluid inclusions therefore suggests that the H_2O–CO_2-rich fluids infiltrating the San Andreas system may also be partially derived from the mantle. To test this hypothesis, Fig. 6 is a plot of the carbon isotopic composition of calcite as a function of the fluid inclusion helium isotope composition for those samples for which a reliable comparison can be made. Although the data are somewhat scattered, in general increasing helium isotope compositions are correlated with decreasing $\delta^{13}C$. The correlation is especially good for the Little Pine Fault (SYF) samples. Since there are no reasonable processes or scenarios that might result in a correlation between cosmogenic [3]He and $\delta^{13}C$, we have labeled this correlation as the Mantle trend line, suggesting that part of the infiltrating CO_2 responsible for the carbon-isotope shifts in veins and deformation zones is derived from the mantle. The scatter in the data likely
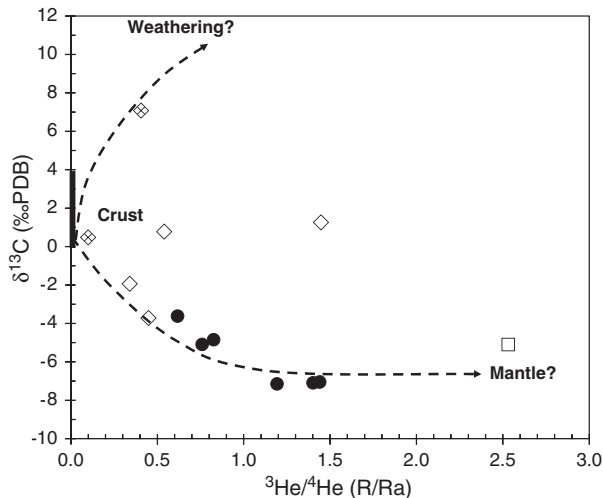

Fig. 6. Helium isotope ratios (R/Ra) from fluid inclusions versus carbon-isotope compositions of their host calcites or of carbonates associated with their host quartz (data from Tables 1 and 2). The solid field along the ordinate axis represents the composition of a typical pristine crustal limestone (R/Ra~0.02 and $\delta^{13}C$~0–4‰, e. g. Veizer, 1983). The dashed lines represent hypothetical trends depicting the impact on the isotope compositions due to weathering or due to the addition of mantle-derived helium and CO_2 with some crustal metamorphic CO_2 contributions. Black dots: LP samples, Little Pine Fault, Santa Ynez subsystem; diamonds: CLP, CPBC, PK and SK samples (with a cross when weathered), San Andreas Fault; square: HF6 sample, San Gabriel Fault.

indicates the influence of other parameters, such as differences in host lithologies, fluid history, weathering and perhaps minor contribution from cosmogenic [3]He production.

It appears from the Mantle trend line in Fig. 6 that the CO_2 infiltrating the SAF system is a mixture of mantle and crustal-derived CO_2. This is consistent with CO_2/[3]He ratios observed in present-day surface springs and wells that were found to be significantly greater (>1000 times) than the canonical mantle value (~10^{10}, Marty and Jambon, 1987), requiring an additional non-mantle-derived CO_2 component (Kennedy et al., 1997). Unfortunately, we could not measure nor can we calculate the fluid inclusion CO_2/[3]He ratio and therefore, it is not possible to estimate the proportions of mantle and crustal-derived CO_2 from the Mantle trend line in Fig. 6. However, it is apparent that in some cases the crustal CO_2 contribution could be as high as ~100%. For illustrative purpose, a second hypothetical trend line is drawn to capture the weathered, carbonate-poor samples PK2 and PK8 (Tables 1 and 2). This trend line assumes that weathering will add an atmospheric component driving the [3]He/[4]He ratio towards 1.0 Ra, with increasing $\delta^{13}C$ (see Fig. 4).

5.4. Fluid regime and structure of the San Andreas Fault

The evidence for mantle helium in fluid inclusions from faulted rocks suggests that the San Andreas Fault system is, in some fashion, linked to the mantle. Prior studies of other continental strike-slip systems (Pili et al., 1997a,b) suggest that such large shear zone systems could possibly have mantle roots. Furthermore, Henstock et al. (1997) and Zhu (2000) describe evidence for vertical offsets of the Moho under the San Andreas Fault, and Yan and Clayton (2007) found a notch structure on the Moho beneath the Eastern San Gabriel Mountains. Teyssier and Tikoff (1998), from seismic anisotropy and rheology, pictured a vertical lithospheric structure for the SAF, and Titus et al. (2007) provided petrological evidence in xenoliths for the continuation of the SAF system into the upper mantle. Shelly et al. (2009) and Peng et al. (2009) suggested that at least a portion of the non volcanic tremors occurs on the deep extension of the fault, at Moho depth, most likely due to near-lithostatic fluid pressure. We also suggest that fluid infiltration from depth could be related to tremor triggering and evolution along the SAF, supporting Nadeau and Guilhem (2009) hypothesis.

Becken et al. (2008), from a magnetotelluric profile across the San Andreas Fault (SAF) near Parkfield observed a steeply dipping upper crustal high-conductivity zone flanking the seismically defined SAF. This zone widens into the lower crust and appears to be connected to a broad conductivity anomaly in the upper mantle, that may represent a deep-rooted channel for crustal and/or mantle fluid ascent. However, Becken et al. (2008) suggest that the SAF does not act as a major fluid pathway. As we draw our conclusions from rocks sampled at the surface along the trace of the SAF, we cannot infer if the identified fluid pathways correspond with the seismically defined fault plane. Most likely, fluid channeling corresponded with high-deformation zones, including pressure solution and crack filling (Pili et al., 2002; Gratier et al., 2003), which may be more active during interseismic intervals rather than during earthquakes.

Infiltration of both CO_2 and H_2O fluids, of both mantle and crustal origins, has not yet been taken into account in numerical models pertaining to earthquake cycles. Faulkner and Rutter (2001) estimated that the flux over time of only mantle-derived CO_2 and water produced from dehydration reactions appears inadequate. A crustal source of fluid and matter has been taken into account by Gratier et al. (2003) who integrated crack sealing by pressure solution and compaction processes. Fulton and Saffer (2009) evaluated the role of water derived from dehydration of a serpentinized mantle wedge in weakening the SAF but neglected CO_2 influx. Overall, metamorphic contributions at the crustal level have been mainly overlooked. As discussed by Kennedy et al. (1997), the helium isotopic composition of SAF surface fluids suggested

mantle-to-surface flow rates of geo-pressured fluids capable of weakening the fault at seismogenic depths. However, assuming a mantle $CO_2/^3He$ ratio for the upwelling fluids, the corresponding flux of mantle CO_2 through the fault (~0.02 g m^{-2} d^{-1}) was probably not adequate for re-generating fault weakening fluid pressures on a time scale defined by SAF earthquake cycles (~100 years), which would require CO_2 fluxes of the order of ~1 g m^{-2} d^{-1} (Kharaka et al., 1999). The additional flux of crustal metamorphic CO_2 (and perhaps H_2O) as found in the present study is of prime interest in the quest for the origin of fluids in the San Andreas Fault system and the ability of the infiltrating fluids to influence fault zone mechanics. The local fluid productions and the mantle fluid flow should be taken into account for assessing the recurrence time needed to rebuild pressure during the seismic cycle.

6. Conclusion

The rocks exposed along the San Andreas Fault system contain a record of fluid–rock interactions associated with faulting. H_2O–CO_2 mixtures focused into relatively narrow fault zones flowed in sufficient quantities to leave a detectable imprint on host rocks, veins and deformation zones. These fluids flow upwards and bear isotope characteristics of deep sources, including contributions from the mantle and metamorphic devolatilization. We confirmed that faults maintain a high permeability due to veins and deformation zones (gouges, cataclasites, mylonites...) and that there is supply of fluids near the ductile roots of crustal fault zones, as theoretically established by Rice (1992). The present study pointed out the multiple reservoirs responsible for fluid infiltration into the San Andreas Fault system. Supply of CO_2 and H_2O from crustal metamorphism must not be neglected and may well represent the missing fluid contribution required to sustain high fault fluid pressures (Kennedy et al., 1997).

The Santa Ynez, the San Andreas, and the San Gabriel fault systems provide a section in depth from the shallow to the lower crust. This depth profile is recorded both by mantle He contributions and the carbon- and oxygen-isotopes (Fig. 3). Fluids are principally metamorphic in origin, coming at each crustal level "from below". An additional mantle fluid contribution (up to a minimum of 35% He) has been found in past fluids of the San Andreas Fault system. A similar contribution has been found in present-day ground waters associated with the faults (Kennedy et al., 1997). Pathways may have been at play for millions of years. In both cases, mantle He fluxes have been sufficiently high not to be erased by the crustal radiogenic ^4He contribution. Long-lived links of the San Andreas Fault system with the mantle underneath and/or high mantle fluid fluxes are suspected. Meteoric water does not appear to be a significant part of the fluid infiltrations and has only been identified in association with late weathering on exposed rock surfaces. Fluid sources are potentially located all along the San Andreas Fault, from bottom to top. The fault system is expected to be a lithospheric structure rooted in the mantle. For fault segments suspected to be particularly hazardous, the potential of their host lithology to produce metamorphic fluids should be evaluated in order to take into account the role of possible fluid infiltrations in triggering a seismic event. The local fluid productions and the mantle fluid flow should be taken into account for assessing the recurrence time needed to rebuild pressure during the seismic cycle. Non-volcanic tremor identified along some segments of the SAF may well result from this complex fluid activity.

Acknowledgments

References

Albarède, F., 1995. Introduction to Geochemical Modeling. Cambridge University Press, Cambridge. 543 pp.

Ali, S., Stute, M., Torgersen, T., Winckler, G., Kennedy, B.M., 2010. Helium measurements of pore fluids obtained from the San Andreas Fault Observatory at Depth (SAFOD, USA) drill cores. Hydrogeology Journal, 1–11. doi:10.1007/s10040-010-0645-6.

Anderson, J.L., Osborne, R.H., Palmer, D.F., 1983. Cataclastic rocks of the San Gabriel fault —an expression of deformation at deeper crustal levels in the San Andreas Fault Zone. Tectonophysics 98, 209–251.

Ballentine, C.J., Burgess, R., Marty, B., 2002. Tracing fluid origin, transport and interaction in the crust, in noble gases in geochemistry and cosmochemistry. In: Porcelli, D., Ballentine, C.J., Weiler, R. (Eds.), Reviews in Mineralogy and Geochemistry, vol. 47. The Mineralogical Society of America, Washington, D.C, pp. 539–614.

Becken, M., et al., 2008. A deep crustal fluid channel into the San Andreas Fault System near Parkfield, California. Geophysical Journal International 173 (2), 718–732.

Brook, E.J., Kurz, M.D., 1993. Surface-exposure chronology using in-situ cosmogenic He-3 in Antarctic quartz sandstone boulders. Quaternary Research 39, 1–10.

Byerlee, J.D., 1990. Friction, overpressure and fault normal compression. Geophysical Research Letters 17.

Chester, F.M., Evans, J.P., Biegel, R.L., 1993. Internal structure and weakening mechanisms of the San Andreas fault. Journal of Geophysical Research 98 (B1), 771–786.

Dibblee, T.W., 1966. Geology of the Central Santa Ynez Mountains, Santa Barbara County, California. California Division of Mines and Geology Bulletin, vol. 186. California Division of Mines and Geology, San Francisco. 99 pp.

Dodson, A., Kennedy, B.M., DePaolo, D.J., 1997. Helium and neon isotopes in the Imnaha Basalt, Columbia River Basalt Group: evidence for a Yellowstone plume source. Earth and Planetary Science Letters 150, 443–451.

Erzinger, J., Wiersberg, T., Dahms, E., 2004. Real-time mud gas logging during drilling of the SAFOD Pilot Hole in Parkfield, CA - art. no. L13S18. Geophysical Research Letters 31 (15) S1318-S1318.

Evans, J.P., Chester, F.M., 1995. Fluid–rock interaction in faults of the San Andreas system: inference from San Gabriel fault rock chemistry and microstructures. Journal of Geophysical Research 100 (B7), 13,007–13,020.

Faulkner, D.R., Rutter, E.H., 2001. Can the maintenance of overpressured fluids in large strike-slip fault zones explain their apparent weakness? Geology 29 (6), 503–506.

Friedman, I., O'Neil, J.R., 1977. Compilation of stable isotope fractionation factors of geochemical interest, In: Fleisher, M. (Ed.), Data of geochemistry, Sixth edition. Geological Survey Professional Paper. United States Government Printing Office, Washington. chapter KK. 115 pp.

Fulton, P.M., Saffer, D.M., 2009. Potential role of mantle-derived fluids in weakening the San Andreas Fault. Journal of Geophysical Research 114.

Gratier, J.-P., Favreau, P., Renard, F., 2003. Modeling fluid transfer along California faults when integrating pressure solution crack sealing and compaction processes. Journal of Geophysical Research 108 (B2).

Henstock, T., Levander, A., Hole, J.A., 1997. Deformation in the lower crust of the San Andreas Fault System in northern California. Science 278, 650–653.

Hickman, S., Sibson, R., Bruhn, R., 1995. Introduction to special section: mechanical involvement of fluids in faulting. Journal of Geophysical Research 100 (B7), 12,831–12,840.

Hickman, S., Zoback, M., Ellsworth, W., 2004. Introduction to special section: preparing for the San Andreas Fault Observatory at Depth. Geophysical Research Letters 31 (12).

Irwin, W.P., Barnes, I., 1975. Effect of geologic structure and metamorphic fluids on seismic behavior of San Andreas fault system in central and northern California. Geology 3 (12), 713–716.

Javoy, M., Pineau, F., Delorme, H., 1986. Carbon and nitrogen isotopes in the mantle. Chemical Geology 57, 41–62.

Johnson, P.A., McEvily, T.V., 1995. Parkfield seismicity: fluid driven? Journal of Geophysical Research 100 (B7), 12,937–12,950.

Kennedy, B.M., et al., 1997. Mantle fluids in the San Andreas fault system, California. Science 278, 1278–1281.

Kharaka, Y.K., Thordsen, J.J., Evans, W.C., 1999. Crustal fluids: CO_2 of mantle and crustal origins in the San Andreas fault system, California. In: Armannsson, H. (Ed.), Geochemistry of the Earth's Surface. Balkema, Rotterdam, pp. 515–518.

Kita, I., Matsuo, S., Wakita, H., 1982. H_2 generation by reaction between H_2O and crushed rock: an experimental study on H_2 degassing from the active fault zone. Journal of Geophysical Research 87 (B13), 10789–10795.

Kulongoski, J.T., Hilton, D.R., Izbicki, J.A., 2003. Helium isotope studies in the Mojave Desert, California: implications for groundwater chronology and regional seismicity. Chemical Geology 202 (1–2), 95–113.

Lewicki, J.L., Brantley, S.L., 2000. CO_2 degassing along the San Andreas fault, Parkfield, California. Geophysical Research Letters 27 (1), 5–8.

Magaritz, M., Taylor Jr., H.P., 1976. Oxygen, hydrogen and carbon isotope studies of the Franciscan formation, Coast Ranges, California. Geochimica et Cosmochimica Acta 40, 215–234.

Marty, B., Jambon, A., 1987. C/3He in volatile fluxes from solid Earth: implications for carbon geodynamics. Earth and Planetary Science Letters 83, 16–26.

Melchiorre, E.B., Criss, R.E., Davisson, M.L., 1999. Relationship between seismicity and subsurface fluids, central Coast ranges, California. Journal of Geophysical Research B1 (104), 921–939.

Moore, D.E., Rymer, M.J., 2007. Talc-bearing serpentinite and the creeping section of the San Andreas fault. Nature 448 (7155), 795–797.

Nadeau, R.M., Guilhem, A., 2009. Nonvolcanic tremor evolution and the San Simeon and Parkfield, California, Earthquakes. Science 325 (5937), 191–193.

O'Neil, J.R., 1984. Water-rock interactions in fault gouge. Pure and Applied Geophysics 122 (2), 440–446.

O'Neil, J.R., Hanks, T., 1980. Geochemical evidence for water-rock interaction along the San Andreas and Garlock faults of California. Journal of Geophysical Research 85 (11), 6286–6292.

O'Neil, J.R., Clayton, R.N., Mayeda, T.K., 1969. Oxygen isotope fractionation in divalent metal carbonates. Journal of Chemical Physics 51, 5547–5558.

Peng, Z., Vidale, J.E., Wech, A.G., Nadeau, R.M., Creager, K.C., 2009. Remote triggering of tremor along the San Andreas Fault in central California. Journal of Geophysical Research 114.

Pik, R., Marty, B., 2009. Helium isotopic signature of modern and fossil fluids associated with the Corinth rift fault zone (Greece): implication for fault connectivity in the lower crust. Chemical Geology 266, 67–75.

Pili, E., Ricard, Y., Lardeaux, J.M., Sheppard, S.M.F., 1997a. Lithospheric shear zones and mantle-crust connections. Tectonophysics 280 (1–2), 15–29.

Pili, E., Sheppard, S.M.F., Lardeaux, J.M., Martelat, J.E., Nicollet, C., 1997b. Fluid flow vs. scale of shear zones in the lower continental crust and the granulite paradox. Geology 25 (1), 15–18.

Pili, E., Poitrasson, F., Gratier, J.P., 2002. Carbon-oxygen isotope and trace element constraints on how fluids percolate faulted limestones from the San Andreas Fault system: partitioning of fluid sources and pathways. Chemical Geology 190 (1–4), 229–248.

Polyak, B.G., et al., 2000. Helium isotopes, tectonics and heat flow in the Northern Caucasus. Geochimica et Cosmochimica Acta 64 (11), 1925–1944.

Rice, J.R., 1992. Fault stress, pore pressure distribution, and the weakness of the San Andreas fault. In: Evans, B., Wong, T.-F. (Eds.), Fault mechanics and transport properties of rocks. : International Geophysics Series. Academic Press, London, pp. 475–503.

Scholz, C.H., 2000. A fault in the 'weak San Andreas' theory. Nature 406 (6793) 234–234.

Sharma, T., Clayton, R.N., 1965. Measurement of 18O/16O ratios of total oxygen of carbonates. Geochimica et Cosmochimica Acta 29, 1347–1353.

Shelly, D.R., Ellsworth, W.L., Ryberg, T., Haberland, C., Fuis, G.S., Murphy, J., Nadeau, R.M., Bürgmann, R., 2009. Precise location of San Andreas Fault tremors near Cholame, California using seismometer clusters: slip on the deep extension of the fault? Geophysical Research Letter 36.

Shimamoto, T., Takemura, K., Fujimoto, K., Tanaka, H., Wibberley, C.A.J., 2001. Part II: Nojima Fault Zone probing by core analyses. Island Arc 10 (3–4), 357–359.

Stuart, F., Turner, G., Taylor, R., 1994. He-Ar isotope systematics of fluid inclusions: resolving mantle and crustal contributions to hydrothermal fluids. In: Matsuda, J. (Ed.), Noble gas geochemistry and cosmochemistry. Terra Scientific Publishing Company, Tokyo, pp. 261–277.

Sugisaki, R., Anno, H., Adachi, M., Ui, H., 1980. Geochemical features of gases and rocks along active faults. Geochemical Journal 14, 101–112.

Teyssier, C., Tikoff, B., 1998. Strike-slip partitioned transpression of the San Andreas fault system: a lithospheric-scale approach. In: Holdsworth, R.E., Strachan, R.A., Dewey, J.F. (Eds.), Continental transpression and transtension tectonics. Geological Society of London Special Publication. Geological Society of London, London, pp. 143–158.

Titus, S.J., Medaris, L.G., Wang, H.F., Tikoff, B., 2007. Continuation of the San Andreas fault system into the upper mantle: evidence from spinel peridotite xenoliths in the Coyote Lake basalt, central California. Tectonophysics 429 (1–2), 1–20.

Toutain, J.P., Baubron, J.-C., 1999. Gas geochemistry and seismotectonics: a review. Tectonophysics 304, 1–27.

Unsworth, M.J., Malin, P.E., Egbert, G.D., Booker, J.R., 1997. Internal structure of the San Andreas fault at Parkfield, California. Geology 25 (4), 359–362.

Veizer, J., 1983. Trace elements and isotopes in sedimentary carbonates. In: Reeder, R.J. (Ed.), Carbonates: mineralogy and chemistry. Mineralogical Society of America, Washington.

Vermeesch, P., Baur, H., Heber, V.S., Kober, F., Oberholzer, P., Schaefer, J.M., Schlüchter, C., Strasky, S., Wieler, R., 2009. Cosmogenic 3He and 21Ne measured in quartz targets after one year of exposure in the Swiss Alps. Earth and Planetary Science Letters 284, 417–425.

Wallace, R.E. (Ed.), 1990. The San Andreas Fault System, California, 1515. US Government Printing Office, Washington. 283 pp.

White, D.E., Barnes, I., O'Neil, J.R., 1973. Thermal and mineral waters of nonmeteoric origin, California Coast Ranges. Geological Society of America Bulletin 84, 547–559.

Wiersberg, T., Erzinger, J., 2007. A helium isotope cross-section study through the San Andreas Fault at seismogenic depths. Geochemistry Geophysics Geosystems 8.

Wiersberg, T., Erzinger, J., 2008. Origin and spatial distribution of gas at seismogenic depths of the San Andreas Fault from drill-mud gas analysis. Applied Geochemistry 23 (6), 1675–1690.

Yan, Z.M., Clayton, R.W., 2007. A notch structure on the Moho beneath the Eastern San Gabriel Mountains. Earth and Planetary Science Letters 260 (3–4), 570–581.

Zhao, D., Kanamori, H., Humphreys, E., 1996. Simultaneous inversion of local and teleseismic data for the crust and mantle structure of southern California. Physics of the Earth and Planetary Interiors 93 (3–4), 191–214.

Zhu, L., 2000. Crustal structure across the San Andreas fault, southern California from teleseismic converted waves. Earth and Planetary Science Letters 179, 183–190.

Zoback, M.D., 2000. Strength of the San Andreas. Nature 405, 31–32.

Zoback, M.D., Zoback, M.L., Mount, V.S., Suppe, J., Eaton, J.P., Healy, J.H., Oppenheimer, D., Reasenberg, P., Jones, L., Raleigh, C.B., Wong, I.G., Scotti, O., Wentworth, C., 1987. New evidence on the state of stress of the San-Andreas Fault system. Science 238, 1105–1111.